TU Delft

Delft University of Technology

Optomechanical methodology for characterizing the thermal properties of 2D materials

Liu, Hanqing; Brahmi, Hatem; Boix-Constant, Carla; van der Zant, Herre S.J.; Steeneken, Peter G.; Verbiest, Gerard J.

DOI
10.1063/5.0190680

Publication date
2024

Document Version
Final published version

Published in
APL Materials

Citation (APA)
Liu, H., Brahmi, H., Boix-Constant, C., van der Zant, H. S. J., Steeneken, P. G., & Verbiest, G. J. (2024). Optomechanical methodology for characterizing the thermal properties of 2D materials. *APL Materials*, *12*(2), Article 021126. https://doi.org/10.1063/5.0190680

Important note
To cite this publication, please use the final published version (if applicable).
Please check the document version above.

Copyright
Other than for strictly personal use, it is not permitted to download, forward or distribute the text or part of it, without the consent of the author(s) and/or copyright holder(s), unless the work is under an open content license such as Creative Commons.

Takedown policy
Please contact us and provide details if you believe this document breaches copyrights.
We will remove access to the work immediately and investigate your claim.

This work is downloaded from Delft University of Technology.
For technical reasons the number of authors shown on this cover page is limited to a maximum of 10.

APL Materials

RESEARCH ARTICLE | FEBRUARY 26 2024

Optomechanical methodology for characterizing the thermal properties of 2D materials

Hanqing Liu ; Hatem Brahmi; Carla Boix-Constant ; Herre S. J. van der Zant ; Peter G. Steeneken ; Gerard J. Verbiest

Check for updates

APL Mater. 12, 021126 (2024)
https://doi.org/10.1063/5.0190680

View Online
Export Citation
CrossMark

08 March 2024 14:14:06

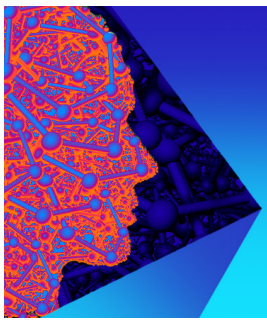
APL Materials
Special Topic: 2D Materials for Biomedical Applications
Submit Today
AIP Publishing

AIP Publishing

Optomechanical methodology for characterizing the thermal properties of 2D materials

Cite as: APL Mater. 12, 021126 (2024); doi: 10.1063/5.0190680
Submitted: 7 December 2023 • Accepted: 24 January 2024 •
Published Online: 26 February 2024

View Online Export Citation CrossMark

Hanqing Liu,[1,a)] Hatem Brahmi,[2] Carla Boix-Constant,[3] Herre S. J. van der Zant,[4] Peter G. Steeneken,[1,4] and Gerard J. Verbiest[1,a)]

AFFILIATIONS

[1] Department of Precision and Microsystems Engineering, Delft University of Technology, Lorentzweg 1, 2628 CD Delft, The Netherlands
[2] ASML Netherlands, B.V., 5504 DR Veldhoven, The Netherlands
[3] Instituto de Ciencia Molecular (ICMol), Universitat de Valencia, Paterna 46980, Spain
[4] Kavli Institute of Nanoscience, Delft University of Technology, 2628 CJ Delft, The Netherlands

[a)] **Author to whom correspondence should be addressed:** H.Liu-7@tudelft.nl and g.j.verbiest@tudelft.nl

ABSTRACT

Heat transport in two dimensions is fundamentally different from that in three dimensions. As a consequence, the thermal properties of 2D materials are of great interest, from both scientific and application points of view. However, few techniques are available for the accurate determination of these properties in ultrathin suspended membranes. Here, we present an optomechanical methodology for extracting the thermal expansion coefficient, specific heat, and thermal conductivity of ultrathin membranes made of 2H-TaS_2, $FePS_3$, polycrystalline silicon, MoS_2, and WSe_2. The obtained thermal properties are in good agreement with the values reported in the literature for the same materials. Our work provides an optomechanical method for determining the thermal properties of ultrathin suspended membranes, which are difficult to measure otherwise. It provides a route toward improving our understanding of heat transport in the 2D limit and facilitates engineering of 2D structures with a dedicated thermal performance.

© 2024 Author(s). All article content, except where otherwise noted, is licensed under a Creative Commons Attribution (CC BY) license (http://creativecommons.org/licenses/by/4.0/). https://doi.org/10.1063/5.0190680

08 March 2024 14:14:06

I. INTRODUCTION

Soon after the discovery of monolayer graphene, it was found that 2D materials have unique thermal properties, which opened opportunities for heat control at the nanoscale.[1–7] Due to their ultrasmall thickness, the thermal properties of 2D materials are dominated by surface scattering of acoustic phonons, which is highly sensitive to strain,[8] grain size,[9] and temperature,[10] as well as material imperfections, such as defects and impurities.[11] To understand and optimize heat transport in 2D materials, precise thermal characterization methods are of great importance.

So far, a variety of experimental techniques have been developed to characterize thermal transport in 2D materials, of which the transient micro-bridge method[12,13] and the steady-state optothermal method based on Raman microscopy are the most commonly used.[14–16] However, the construction of a micro-bridge is complicated and thermal contact resistances can affect measurement results, while for Raman measurements, the probed temperature resolution is usually relatively small, leading to large error bars. These limitations undermine the accuracy of probing heat transport in 2D materials, causing large variations in the thermal material parameters reported in the literature. For example, literature values for the thermal conductivity vary from 2000 to 5000 W m^{-1} K^{-1} for suspended monolayer graphene.[17] Recently, optomechanical measurement has been used for characterizing the heat transport on the $MoSe_2$ membrane.[18] However, the presented method is less involved as it requires tuning the laser power, inducing electrostatic strain, and calibrating the temperature distribution on the membrane with respect to the laser spot size.

In this work, we demonstrate an optomechanical non-contact method for measuring the thermal properties of nanomechanical resonators made of free-standing 2D materials. The presented methodology allows us to simultaneously extract the thermal expansion coefficient, the specific heat, and the in-plane thermal conduc-

© Author(s) 2024

tivity of the material. It involves driving a suspended membrane using a power-modulated laser and measuring its time-dependent deflection with a second laser. Thus, both the temperature-dependent mechanical fundamental resonance frequency of the membrane and characteristic thermal time constant at which the membrane cools down[19] are measured. A major advantage of the method is that no physical contact needs to be made with the membrane such that its pristine properties are probed and no complex device fabrication is needed. Buckling effects are incorporated in the model to account for the induced compressive stress during temperature variations. Our results on 2H-TaS_2, $FePS_3$, polycrystalline silicon (poly-Si), MoS_2, and WSe_2 show good agreement with reported values in the literature.

II. FABRICATION AND METHODOLOGY

We fabricate 2D nanomechanical resonators by transferring 2D flakes over circular cavities with a depth of 285 nm and a radius R of 3–4 μm in a silicon (Si) substrate with a 285 nm thick silicon oxide (SiO_2) layer, as illustrated in Fig. 1(a). The devices D1–D5 studied in this work are made of 2H-TaS_2, $FePS_3$, poly-Si, MoS_2, and WSe_2, respectively. By using a tapping mode atomic force microscope (AFM), we determine the thickness, h, of each membrane (see Table I). All details about the device fabrication and thickness measurement can be found in the supplementary material, Sec. 1. To determine Young's modulus E of each membrane, we use the AFM to indent the center of the suspended area with a force F while measuring the cantilever indentation δ.[20] The measured F vs δ, as depicted in Fig. 1(b) for device D1, is fitted with a model for point-force loading of a circular plate given by $F = (\frac{16\pi D}{R^2}\delta) + n_0\pi\delta + Ehq^3(\frac{\delta^3}{R^2})$, where $D = Eh^3/(12(1-\nu^2))$ is the bending rigidity of the membrane, ν is the Poisson ratio, $n_0 = Eh\varepsilon_0/(1-\nu)$ is the initial tension in the membrane, and ε_0 is the prestrain. We extract E = 108.45 GPa and $\varepsilon_0 = 6.75 \times 10^{-3}$ from the fit shown in Fig. 1(b) (drawn line), which are in good agreement with the typical values found in the literature for 2H-TaS_2.[21] The obtained values of E for devices D2–D5 are listed in Table I.

The setup for the optomechanical measurement[27,28] is shown in Fig. 1(c). A power-modulated blue diode laser (λ = 405 nm) photothermally actuates the resonator, while a He–Ne laser (λ = 632 nm), of which the reflected laser power depends on the position of the membrane, is used to detect the motion of the resonator. The power-modulation of the blue laser is supplied by using a Vector Network Analyzer (VNA), which also analyzes the photodiode signal containing the reflected laser power and converts that to the response amplitude, $|z_f|$, of the resonator in the frequency

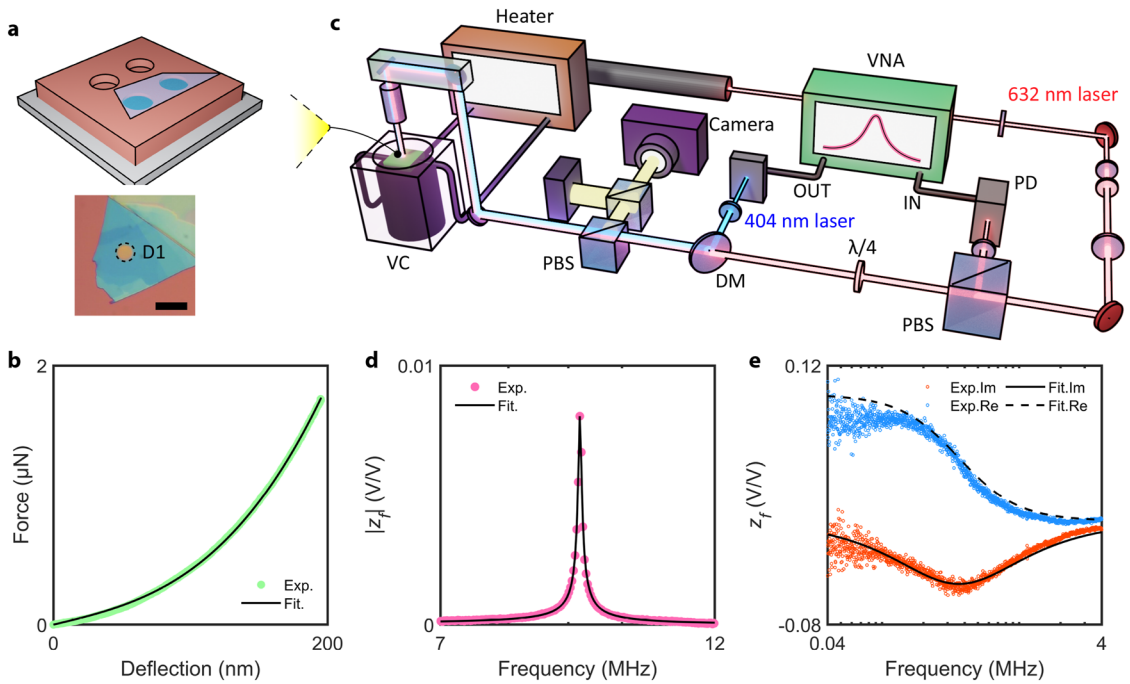

FIG. 1. Sample characterization and experimental setup. (a) Top, schematic diagram of 2D nanomechanical resonators, composed of a 2D flake suspended on the etched SiO_2/Si cavities; bottom, optical image of device D1 (2H-TaS_2). The scale bar is 5 μm. (b) AFM indentation results for device D1 (points), from which Young's modulus E of the membrane is extracted by fitting the measured force F to the cantilever deflection δ (drawn line). (c) Laser interferometry setup used for the optomechanical measurement. The sample is mounted in a vacuum chamber (VC) with a pressure below 10^{-5} mbar. The reflected red laser is detected by the photodiode (PD) and input into the vector network analyzer (VNA). PBS, polarized beam splitter; DM, Dirac mirror. (d) Resonant peak of device D1 measured at the MHz regime (points), which is fitted with a harmonic model (drawn line) to extract the fundamental resonance frequency f_0 of device D1. (e) Thermal signal measured at the kHz regime, including imaginary (red points) and real (blue points) parts. The imaginary part is fitted with Eq. (1) (drawn lines) to obtain the thermal time constant τ of device D1.

08 March 2024 14:14:06

© Author(s) 2024

TABLE I. Characteristics of devices D1–D5, including radius R, thickness h, mass density ρ, Young's modulus E, atomic mass M, Poisson ratio ν, and Grüneisen parameter γ, and the obtained average TEC α_m, specific heat C_v, and in-plane thermal conductivity k. The values of ρ, M, ν, and γ are taken from the literature.[21–26]

	R (μm)	h (nm)	ρ (kg m^{-3})	E (GPa)	M (g mol^{-1})	ν	γ	α_m ($\times 10^{-6}$ K^{-1})	C_v (J mol^{-1} K^{-1})	k (W m^{-1} K^{-1})
D1 (2H-TaS_2)	4	23.2	6860	108.45	245	0.35	2.13	6.96	42.0	8.6
D2 ($FePS_3$)	4	33.9	3375	69.60	183	0.304	1.80	12.7	68.2	1.8
D3 (poly-Si)	4	24.0	2330	140.52	28	0.22	0.45	3.10	20.7	5.3
D4 (MoS_2)	3	4.8	5060	174.32	160	0.25	0.41	3.37	90.6	28.8
D5 (WSe_2)	3	5.5	9320	94.42	342	0.19	0.79	7.63	53.8	11.0

domain. All measurements were done in vacuum at a pressure below 10^{-5} mbar. As shown in Fig. 1(d), $|z_f|$ shows a clear fundamental resonance peak, which we fit with a harmonic oscillator model given by $|z_f| = \frac{A_{\mathrm{res}} f_0^2}{Q\sqrt{(f_0^2-f^2)^2+(f_0 f/Q)^2}}$, where f_0 is the fundamental resonance frequency, A_{res} is the vibration amplitude at resonance, and Q is the quality factor. For device D1, we obtain an f_0 = 9.53 MHz and Q = 160. In addition, we also find a maximum in the imaginary part of z_f at kHz frequencies [see Fig. 1(e)], which we attribute to the thermal expansion of the membrane that is time-delayed with respect to the modulated blue laser power because it takes a time τ for the temperature of the membrane to rise.[29,30] By solving the in-plane heat equation in the membrane, the thermal signal can be expressed as

$$z_f = \frac{A_{\mathrm{th}}}{i2\pi f\tau + 1}, \tag{1}$$

where A_{th} and τ are the thermal expansion amplitude and thermal time constant of the membrane, respectively. The red and blue laser powers are fixed at 0.9 and 0.13 mW, respectively, to ensure linear vibration of the resonators with a negligible temperature raise of the membrane due to self-heating.[29] We extract τ by fitting the measured imaginary part of z_f to Eq. (1) [see Fig. 1(e)]. Here,

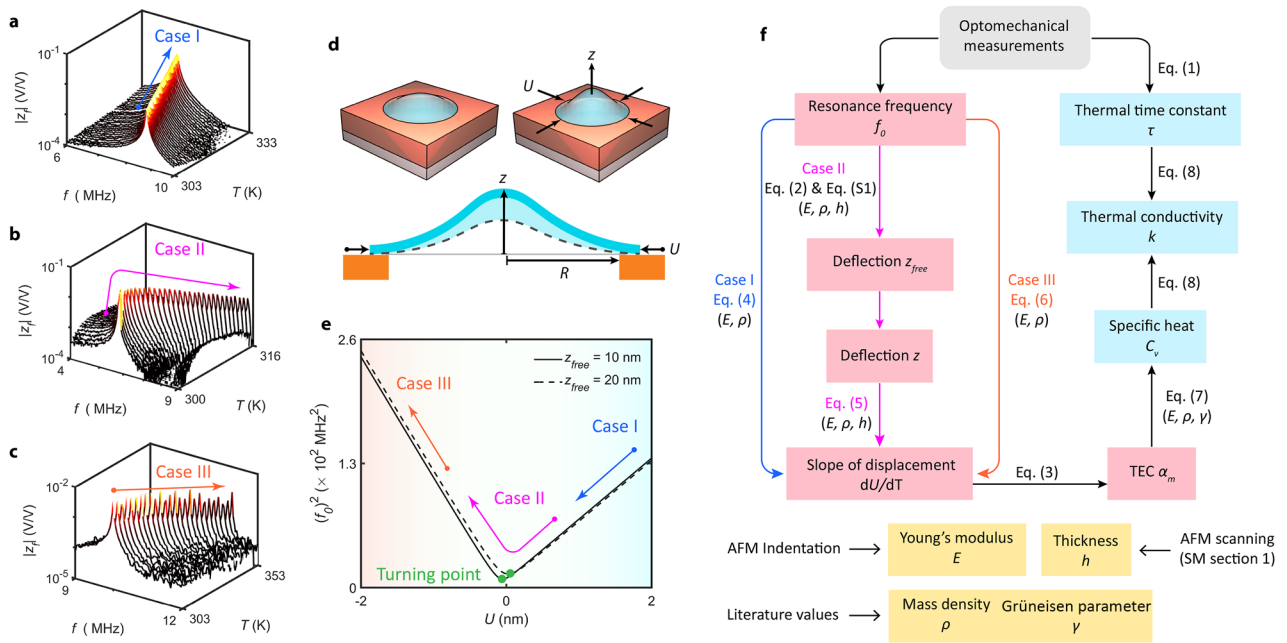

FIG. 2. Optomechanical methodology for obtaining thermal properties. (a)–(c) Resonant peak measured as a function of temperature T for devices D1 to D3, corresponding to cases I to III, respectively. (d) Schematic diagram of the buckled device, where the central deflection z of the membrane increases as the boundary displacement U is loaded. (e) Squared resonance frequency f_0^2 as a function of U in the membrane estimated by Eqs. (2) and (S1) under different z_{free}. f_0^2 first decreases and then increases again as U varies from tensile to compressive, which is comparable to the measurement result for device D2. (f) The proposed procedure to determine thermal properties of 2D material membranes.

08 March 2024 14:14:06

© Author(s) 2024

we obtain the maximum of $\mathrm{Im}(z_f)$ at around 366.19 kHz for device D1, corresponding to $\tau = (2\pi \times 366.19\ \mathrm{kHz})^{-1} = 434.62$ ns.

III. RESULTS

A. Thermally induced buckling phenomenon

When changing the temperature, the thermal expansion coefficient (TEC) α_m of the membrane, which is higher than that of the silicon substrate α_{Si}, changes the strain in the membrane by a quantity $\Delta\varepsilon$. This results in a remarkable change in the dynamics of 2D nanomechanical resonators, which can be used for probing the thermal properties.[31,32] Therefore, we heat up the fabricated devices and investigate the dependence of resonance frequency f_0 on temperature T. As shown in Fig. 2(a), we observe a decrease in f_0 with increasing T for device D1, which is in agreement with trends shown in the literature[33] and can be attributed to a reduction in strain when the material thermally expands. However, the results obtained for devices D2 and D3 are substantially different. As shown in Figs. 2(b) and 2(c), we observe an initial decrease in f_0 with increasing T toward a minimum frequency (which we call the turning point), followed by a continuous increase. We attribute this to the thermally induced buckling of the mechanical resonators as found in earlier studies,[34–36] which is caused by the loaded compression since $\alpha_m > \alpha_{\mathrm{Si}}$. Here, as depicted in Fig. 2(d), the thermal expansion of the membrane causes a compressive stress that triggers the membrane to buckle. We label the pre-buckling, the transition from pre-buckling to post-buckling, and the post-buckling regions in Fig. 2(e) as cases I, II, and III, respectively.

We use the Galerkin model for a clamped circular plate[37,38] to find an approximate analytical expression of the fundamental resonance frequency f_0 under thermally induced buckling,[39]

$$f_0(T) = \frac{10.33h}{\pi d^2}\sqrt{\frac{E}{3\rho(1-\nu^2)}\left(1+\beta(1-\nu^2)\frac{3z^2-z_{free}^2}{h^2}+\frac{3}{8}(1+\nu)\frac{Ud}{h^2}\right)}, \tag{2}$$

where d is the diameter of the plate, U is the thermally changed in-plane displacement from boundary, ρ is the mass density, z is the central deflection of the plate, ν is the Poisson ratio, z_{free} is the central deflection of the plate in the pre-deformed state when $U = 0$ (without loading), and β is a fitting factor determined by[39] $\beta = 0.35\nu + 0.42$. Equation (2) shows that f_0 depends on the in-plane displacement $U(T)$ from the boundary and the central deflection $z(T)$ of the membrane. The relation between $z(T)$ and $U(T)$ can be found in the supplementary material, Sec. 1 [see Eq. (S1)]. Following the literature,[39] z_{free} can be extracted from the measured value of the fundamental resonance frequency at the turning point, f_t, using the built Galerkin model.

By substituting $R = 4\ \mu$m, $h = 23$ nm, $E = 108$ GPa, $\rho = 6860$ kg/m^3, $\nu = 0.35$, and $\beta = 0.54$ into Eqs. (2) and (S1), we obtain f_0^2 vs U as shown in Fig. 2(e). For case I, f_0^2 decreases as U increases, while for cases II and III, z increases as buckling happens [see Fig. S2(b)], leading to an increase in f_0^2. The estimation shown in Fig. 2(e) can thus account for all measured results of f_0 vs T for devices D1 to D3. In the following, we describe how to extract the slope of thermal-changed displacement U vs temperature $\frac{dU}{dT}$ for cases I to III, which is related to the TEC α_m of the membrane through[31]

$$\frac{1}{R}\frac{dU}{dT} = -[\alpha_m(T) - \alpha_{\mathrm{Si}}(T)]. \tag{3}$$

1. Case I. Pre-buckling regime

For case I, the suspended membrane is nearly flat, while the change of deflection z with increasing temperature T can be negligible. Therefore, assuming $\frac{dz}{dT} = 0$, the derivative of Eq. (2) can be simplified as (see the details in supplementary material, Sec. 2)

$$\frac{df_0^2}{dT} = c_t\frac{dU}{dT}, \tag{4}$$

where $c_t = \frac{13.34E}{\pi^2 d^3\rho(1-\nu)}$. Therefore, in the pre-buckling regime, we can directly extract $\frac{dU}{dT}$ from the measured $\frac{df_0^2}{dT}$ using Eq. (4) [see the flow chart in Fig. 2(f)]. In addition to device D1, we also show that devices D4 and D5 are in case I, according to their measured f_0 vs T (see the supplementary material, Sec. 4).

2. Case II. Transition from pre-buckling to post-buckling

For case II, Eq. (4) is not applicable anymore since $z(T)$ varies with temperature. Thus, we calculate the derivative of Eq. (2) (see supplementary material, Sec. 2) and obtain

$$\frac{df_0^2}{dT} = c_t\left(1-\frac{32}{\frac{16}{3\beta(1-\nu^2)}\frac{z_{free}h^2}{z^3}+10.7}\right)\frac{dU}{dT}. \tag{5}$$

As depicted in the flow chart shown in Fig. 2(f), we first extract $z_{free} = 20.6$ nm for device D2 from the measured f_0 at the turning point using Eqs. (2) and (S1), as well as z vs T (see Fig. S2). The obtained z_{free} and $z(T)$ are then substituted into Eq. (5) to extract $\frac{dU}{dT}$. The result of U vs T for device D2 shows the expected transition of displacement from tensile ($U > 0$) to compressive ($U < 0$), as shown in Fig. S2.

3. Case III. Post-buckling regime

For case III, Eq. (5) can be simplified as $z^3 \gg z_{free}h^2$, which results in

$$\frac{df_0^2}{dT} = -2c_t\frac{dU}{dT}. \tag{6}$$

Thus, the result of $\frac{dU}{dT}$ for device D3 can be directly extracted from the measured f_0 vs T. The calculated curves in Fig. 2(e) also verify the linear relations given in Eqs. (4) and (6).

B. Extracting in-plane thermal conductivity of 2D materials

The flow chart depicted in Fig. 2(f) also shows how optomechanical measurements as a function of temperature enable a precise pathway for studying the thermal properties of 2D resonators. We first extract the TEC α_m of the membrane from the results of $\frac{dU}{dT}$ from cases I to III, which are obtained from Eqs. (4)–(6), respectively, as discussed in Sec. III A 3. Then, we quantify the specific heat c_v of

08 March 2024 14:14:06

© Author(s) 2024

the membrane from its thermodynamic relation with α_m, which will be discussed in this section in more detail. Finally, from the solution of the 2D heat equation, we determine the in-plane thermal conductivity k of the membrane from the measured τ and the obtained c_v. In the following, we go through this procedure step by step for device D1.

Let us start with extracting the TEC α_m of the membrane. Since the in-plane displacement U originates from the boundary thermal expansion of the membrane, we can extract the TEC $\alpha_m(T)$ of the membrane from the obtained $\frac{dU}{dT}$ using Eq. (3), where the values of $\alpha_{Si}(T)$ are taken from the literature.[40] The obtained α_m vs T for device D1 is shown in Fig. 3(a) (left).

In the second step, since the specific heat at a constant volume is approximately equal to that at constant pressure for solids, we can directly extract the specific heat, C_v, of the membrane from the TEC α_m using the thermodynamic relation[26]

$$C_v = \frac{3\alpha_m K V_M}{\gamma\rho}, \tag{7}$$

where $K = \frac{E}{3(1-2\nu)}$ is the bulk modulus, $V_M = M/\rho$ is the molar volume, M is the atomic mass, and γ is the Grüneisen parameter of the membrane taken from the literature. These parameters are listed in Table I for the materials used. Using the obtained α_m, we extract C_v vs T for device D1, as shown in Fig. 3(a) (right).

In the last step, we focus on the heat transport in 2D membranes. As shown in Fig. 3(b), we experimentally observe that τ is between 434.6 and 444.0 ns in the probed T range for device D1. Considering the heat transport in a circular membrane, we solve the heat equation in the membrane with an appropriate initial temperature distribution and well-defined boundary conditions (see the supplementary material, Sec. 3) and obtain the thermal time constant based on the thermal properties of the membrane,

$$\tau^{-1} = {\tau_{rr}}^{-1} + {\tau_{zz}}^{-1} = \frac{k}{\rho c_v}\left(\frac{\mu^2}{R^2} + \frac{\pi^2}{4h^2}\right), \tag{8}$$

where τ_{rr} and τ_{zz} are the in-plane and out-of-plane thermal time constants of the membrane [see Fig. 3(b), inset], respectively, $c_v = C_v/M$, $\mu^2 = 5$ is the in-plane diffusive constant (see the supplementary material, Sec. 3), and k is the thermal conductivity of the membrane. Due to the low h/R ratio for 2D materials, we find that $\tau_{zz} \ll \tau_{rr}$ and thus the extracted τ from our measurement is equal to τ_{rr}. By substituting the obtained C_v and the measured τ into Eq. (8), we extract $k = 8.6 \pm 0.3$ W m^{-1} K^{-1} for device D1, as shown in Fig. 3(c).

The obtained in-plane thermal conductivity k for devices D1–D5 is listed in Table I, of which the raw data are presented in Fig. S6. Since relevant studies on the thermal properties of both 2H-TaS_2 (device D1) and $FePS_3$ (device D2) are quite limited, we directly compare the obtained k with the values from the literature[22,43] and observe good agreements (see Fig. 4). For poly-Si (device D3), MoS_2 (device D4), and WSe_2 (device D5), we observe that k depends on the membrane thickness h. We attribute this to a smaller mean free path (MFP) of phonons in thin membranes compared to their bulk counterparts.[10] To account for this effect, we use the Fuchs–Sondheimer

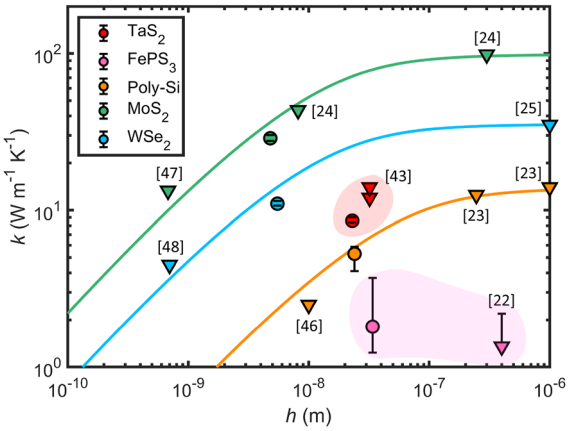

FIG. 4. In-plane thermal conductivity k of 2D material membranes vs their thickness h. Circular points, the obtained k for devices D1–D5 in this work; triangle points, literature values; drawn lines, estimations of k vs h by using the Fuchs–Sondheimer model using Eq. (9).

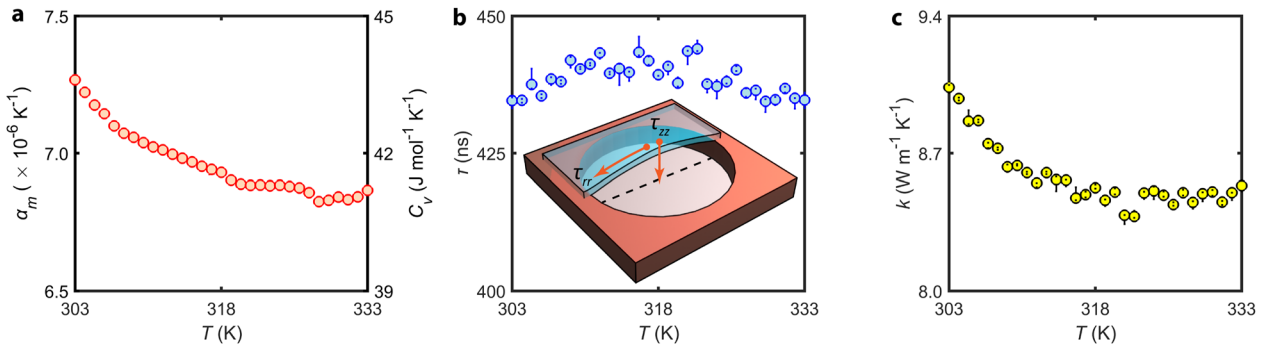

FIG. 3. Quantifying the thermal characteristics of device D1. (a) Thermal expansion coefficient α_m and specific heat C_v of 2H-TaS_2 membrane vs temperature T. (b) Measured thermal time constant τ vs T. The inset is the schematic diagram of heat transport in the suspended 2D membrane. (c) In-plane thermal conductivity k vs T extracted from Eq. (8) using the measured τ and the obtained C_v.

08 March 2024 14:14:06

© Author(s) 2024

model[24,44] that evaluates the thermal conductivity of 2D materials as a function of thickness,

$$\frac{k}{k_{\text{bulk}}} \approx 1 - \frac{3}{8}\frac{\Lambda_{\text{bulk}}}{h} + \frac{3}{2}\frac{\Lambda_{\text{bulk}}}{h}\int_1^\infty \left(\frac{1}{x^3} - \frac{1}{x^5}\right) e^{-\frac{h}{\Lambda_{\text{bulk}}}x}\,dx, \quad (9)$$

where k_{bulk} and Λ_{bulk} are the thermal conductivity and MFP of bulk, respectively, and x is an integration variable. The bulk thermal conductivities k_{bulk} for poly-Si, MoS_2, and WSe_2 are 13.8, 98.5, and 35.3 W m^{-1} K^{-1}, respectively.[23,25,45] We find that the given k vs h, including our results and literature values,[22–25,43,46–48] are well described by Eq. (9) as indicated by the fitted solid lines in Fig. 4 using Λ_{bulk} as the fit parameter, obtaining 75, 19, and 19 nm for poly-Si, MoS_2, and WSe_2, respectively. These fitted values of Λ_{bulk} are also in good agreement with previously reported phonon MFPs,[23,49,50] supporting the validity of employing Eq. (9) to predict the thickness-dependent thermal conductivity of 2D materials.

IV. DISCUSSION

Compared to other methods of determining the thermal conductivity of 2D materials, the optomechanical approach has several advantages, as summarized in Table II. In the Raman microscopy method, since relatively large temperature changes are needed to resolve the resulting shift in the Raman mode frequency, a very wide temperature range has to be measured to get an accurate slope χ_T of the Raman peak shift with temperature. For example, χ_T for MoS_2 is −0.013 cm^{-1}/K. Considering a limited resolution of 0.25 cm^{-1} for a Raman microscope, a temperature increase of at least 20 K is required to obtain meaningful results.[51] In our measurements, we require only a narrow T range to study the thermal transport (see Fig. S6). For the micro-bridge method, either thick crystals or stiff 2D materials, such as graphene, are required to survive the complicated fabrication procedures, including lithography and etching.[2] By contrast, for the presented contactless optomechanical method, one only needs to suspend membranes over cavities in a Si substrate, which is applicable for most 2D materials and can be done for any thickness.

The proposed methodology is applicable to 2D resonators that can be excited photothermally with thermal time constants τ between 160 ns and 16 μs, corresponding to a detection range of thermal signal from 10 kHz to 1 MHz on VNA. Consequently, the thermal expansion coefficient is nonzero and there is a trade-off between the required laser power and resonator thickness. Moreover, the 2D resonator should not be perfectly flat. In reality, inhomogeneities due to uneven adhesion between the membrane and substrate could lead to multiple smaller corrugations and wrinkles superimposed in the membrane when buckling occurs. This potential limitation, which has been observed for suspended 2D resonators before,[52] could result in estimation errors when extracting specific heat from the mechanical buckling model. Moreover,Eq. (8) is not applicable for monolayer and bilayer graphene, in which the scattering of flexural phonons at the boundary between the supported and suspended parts of the 2D material dominates the value of the thermal time constant τ in measurement.[19,28]

Although we estimate the average MFP for bulk in Fig. 4, we note that the phonon MFP in 2D materials is highly related to the phonon dispersion relation, surface strain, crystal grain size, and temperature. These factors significantly affect the thermal characteristics of 2D materials and can be further studied using the presented optomechanical approach, which would help us better understand the phonon scattering mechanisms in 2D materials. Moreover, our work suggests a new way to further investigate acoustic phonon transport in recently emerged 2D materials, such as phosphorene and MXenes with distinct thermal anisotropy,[53,54] as well as the magic-angle multilayer superconductor family.[55] It is also of interest to probe the dynamics of phonons across the interface in vdW heterostructures so as to realize a coherent control of thermal transport across 2D interfaces.[56,57]

TABLE II. Comparison of different thermal conductivity measurement methods, where the required temperature range is quantified by the studies of MoS_2.

	Raman microscopy	Micro-bridge method	Optomechanics
Required range temperature	50–100 K[41,42]	10–50 K[12]	<10 K
Sample preparation	Easy	Difficult	Easy
Applicability to 2D materials	Applicable	Limited	Applicable

V. CONCLUSIONS

We demonstrated an optomechanical approach for probing the thermal transport in 2D nanomechanical resonators made of few-layer 2H-TaS_2, $FePS_3$, poly-Si, MoS_2, and WSe_2. We measured the resonance frequency and thermal time constant of the devices as a function of temperature, which are used to extract their thermal expansion coefficient, specific heat, and in-plane thermal conductivity. The obtained values of all these parameters (see Table I) are in good agreement with the values reported in the literature. Compared to other methods for characterizing the thermal properties of 2D materials, the presented contactless optomechanical approach requires a smaller temperature range, allows for easy sample fabrication, and is applicable to any 2D material. This work not only advances the fundamental understanding of phonon transport in 2D materials but also potentially enables studies into the use of strain engineering and heterostructures for controlling heat flow in 2D materials.

SUPPLEMENTARY MATERIAL

The supplementary material contains the sample fabrication and characterization, mechanical model of 2D material membranes under cases I to III, heat transport model, and raw data of optomechanical measurements for devices D2 to D5.

ACKNOWLEDGMENTS

P.G.S. and G.J.V. acknowledge the support by the Dutch 4TU federation for the Plantenna project. H.S.J.v.d.Z. and P.G.S.

08 March 2024 14:14:06

© Author(s) 2024

acknowledge funding from the European Union's Horizon 2020 research and innovation program under Grant Agreement No. 881603. H.L. acknowledges the financial support from China Scholarship Council. C.B.-C. acknowledges the financial support from the European Union (ERC AdG Mol-2D 788222), the Spanish MICIN (2D-HETEROS PID2020-117152RB-100, co-financed by FEDER, and Excellence Unit "María de Maeztu" CEX2019-000919-M), the Generalitat Valenciana (PROMETEO Program and PO FEDER Program, Ph.D fellowship), and the Advanced Materials program [supported by MCIN with funding from European Union NextGenerationEU (PRTR-C17.I1) and by Generalitat Valenciana].

AUTHOR DECLARATIONS

Conflict of Interest

The authors have no conflicts to disclose.

Author Contributions

Hanqing Liu: Data curation (equal); Investigation (equal); Methodology (equal); Software (equal); Writing – original draft (equal). **Hatem Brahmi**: Formal analysis (equal); Funding acquisition (equal); Writing – review & editing (equal). **Carla Boix-Constant**: Resources (supporting). **Herre S. J. van der Zant**: Funding acquisition (lead); Supervision (supporting); Writing – review & editing (equal). **Peter G. Steeneken**: Formal analysis (equal); Funding acquisition (lead); Methodology (equal); Project administration (equal); Supervision (equal); Writing – review & editing (lead). **Gerard J. Verbiest**: Data curation (equal); Formal analysis (equal); Funding acquisition (equal); Investigation (equal); Supervision (lead); Writing – review & editing (lead).

DATA AVAILABILITY

The data that support the findings of this study are available from the corresponding author upon reasonable request.

REFERENCES

[1]Y. Fu, J. Hansson, Y. Liu, S. Chen, A. Zehri, M. K. Samani, N. Wang, Y. Ni, Y. Zhang, Z. Zhang, Q. Wang, M. Li, H. Lu, M. Sledzinska, C. M. Sotomayor Torres, S. Volz, A. A. Balandin, X. Xu, and J. Liu, "Graphene related materials for thermal management," 2D Mater. **7**, 012001 (2020).

[2]Y. Wang, N. Xu, D. Li, and J. Zhu, "Thermal properties of two dimensional layered materials," Adv. Funct. Mater. **27**, 1604134 (2017).

[3]R. Mas-Balleste, C. Gomez-Navarro, J. Gomez-Herrero, and F. Zamora, "2D materials: To graphene and beyond," Nanoscale **3**, 20–30 (2011).

[4]F. Wu, H. Tian, Y. Shen, Z.-Q. Zhu, Y. Liu, T. Hirtz, R. Wu, G. Gou, Y. Qiao, Y. Yang *et al.*, "High thermal conductivity 2D materials: From theory and engineering to applications," Adv. Mater. Interfaces **9**, 2200409 (2022).

[5]X. Gu and R. Yang, "Phonon transport and thermal conductivity in two-dimensional materials," Annu. Rev. Heat Transfer **19**, 1 (2016).

[6]E. Pop, V. Varshney, and A. K. Roy, "Thermal properties of graphene: Fundamentals and applications," MRS Bull. **37**, 1273–1281 (2012).

[7]A. A. Balandin, "Thermal properties of graphene and nanostructured carbon materials," Nat. Mater. **10**, 569–581 (2011).

[8]H. Liu, G. Qin, Y. Lin, and M. Hu, "Disparate strain dependent thermal conductivity of two-dimensional penta-structures," Nano Lett. **16**, 3831–3842 (2016).

[9]H. Ying, A. Moore, J. Cui, Y. Liu, D. Li, S. Han, Y. Yao, Z. Wang, L. Wang, and S. Chen, "Tailoring the thermal transport properties of monolayer hexagonal boron nitride by grain size engineering," 2D Mater. **7**, 015031 (2019).

[10]Z. Luo, J. Maassen, Y. Deng, Y. Du, R. P. Garrelts, M. S. Lundstrom, P. D. Ye, and X. Xu, "Anisotropic in-plane thermal conductivity observed in few-layer black phosphorus," Nat. Commun. **6**, 8572 (2015).

[11]X. Gu, Y. Wei, X. Yin, B. Li, and R. Yang, "Colloquium: Phononic thermal properties of two-dimensional materials," Rev. Mod. Phys. **90**, 041002 (2018).

[12]I. Jo, M. T. Pettes, E. Ou, W. Wu, and L. Shi, "Basal-plane thermal conductivity of few-layer molybdenum disulfide," Appl. Phys. Lett. **104**, 201902 (2014).

[13]C. Wang, J. Guo, L. Dong, A. Aiyiti, X. Xu, and B. Li, "Superior thermal conductivity in suspended bilayer hexagonal boron nitride," Sci. Rep. **6**, 25334 (2016).

[14]A. A. Balandin, S. Ghosh, W. Bao, I. Calizo, D. Teweldebrhan, F. Miao, and C. N. Lau, "Superior thermal conductivity of single-layer graphene," Nano Lett. **8**, 902–907 (2008).

[15]H. Zhou, J. Zhu, Z. Liu, Z. Yan, X. Fan, J. Lin, G. Wang, Q. Yan, T. Yu, P. M. Ajayan, and J. M. Tour, "High thermal conductivity of suspended few-layer hexagonal boron nitride sheets," Nano Res. **7**, 1232–1240 (2014).

[16]H. Malekpour and A. A. Balandin, "Raman-based technique for measuring thermal conductivity of graphene and related materials," J. Raman Spectrosc. **49**, 106–120 (2018).

[17]D. L. Nika and A. A. Balandin, "Phonons and thermal transport in graphene and graphene-based materials," Rep. Prog. Phys. **80**, 036502 (2017).

[18]N. Morell, S. Tepsic, A. Reserbat-Plantey, A. Cepellotti, M. Manca, I. Epstein, A. Isacsson, X. Marie, F. Mauri, and A. Bachtold, "Optomechanical measurement of thermal transport in two-dimensional $MoSe_2$ lattices," Nano Lett. **19**, 3143–3150 (2019).

[19]R. J. Dolleman, S. Houri, D. Davidovikj, S. J. Cartamil-Bueno, Y. M. Blanter, H. S. van der Zant, and P. G. Steeneken, "Optomechanics for thermal characterization of suspended graphene," Phys. Rev. B **96**, 165421 (2017).

[20]A. Castellanos-Gomez, M. Poot, G. A. Steele, H. S. van der Zant, N. Agraït, and G. Rubio-Bollinger, "Elastic properties of freely suspended MoS_2 nanosheets," Adv. Mater. **24**, 772–775 (2012).

[21]M. Lee, M. Siskins, S. Mañas-Valero, E. Coronado, P. G. Steeneken, and H. S. van der Zant, "Study of charge density waves in suspended 2H-TaS_2 and 2H-$TaSe_2$ by nanomechanical resonance," Appl. Phys. Lett. **118**, 193105 (2021).

[22]F. Kargar, E. A. Coleman, S. Ghosh, J. Lee, M. J. Gomez, Y. Liu, A. S. Magana, Z. Barani, A. Mohammadzadeh, B. Debnath *et al.*, "Phonon and thermal properties of quasi-two-dimensional $FePS_3$ and $MnPS_3$ antiferromagnetic semiconductors," ACS Nano **14**, 2424–2435 (2020).

[23]S. Uma, A. McConnell, M. Asheghi, K. Kurabayashi, and K. Goodson, "Temperature-dependent thermal conductivity of undoped polycrystalline silicon layers," Int. J. Thermophys. **22**, 605–616 (2001).

[24]J. J. Bae, H. Y. Jeong, G. H. Han, J. Kim, H. Kim, M. S. Kim, B. H. Moon, S. C. Lim, and Y. H. Lee, "Thickness-dependent in-plane thermal conductivity of suspended MoS_2 grown by chemical vapor deposition," Nanoscale **9**, 2541–2547 (2017).

[25]S. Kumar and U. Schwingenschlogl, "Thermoelectric response of bulk and monolayer $MoSe_2$ and WSe_2," Chem. Mater. **27**, 1278–1284 (2015).

[26]M. Siskins, M. Lee, S. Mañas-Valero, E. Coronado, Y. M. Blanter, H. S. van der Zant, and P. G. Steeneken, "Magnetic and electronic phase transitions probed by nanomechanical resonators," Nat. Commun. **11**, 2698 (2020).

[27]M. Siskins, E. Sokolovskaya, M. Lee, S. Mañas-Valero, D. Davidovikj, H. S. van der Zant, and P. G. Steeneken, "Tunable strong coupling of mechanical resonance between spatially separated $FePS_3$ nanodrums," Nano Letters **22**, 36–42 (2021).

[28]H. Liu, M. Lee, M. Šiškins, H. van der Zant, P. Steeneken, and G. Verbiest, "Tuning heat transport in graphene by tension," Phys. Rev. B **108**, L081401 (2023).

[29]R. J. Dolleman, D. Lloyd, M. Lee, J. S. Bunch, H. S. van der Zant, and P. G. Steeneken, "Transient thermal characterization of suspended monolayer MoS_2," Phys. Rev. Mater. **2**, 114008 (2018).

[30]R. J. Dolleman, G. J. Verbiest, Y. M. Blanter, H. S. van der Zant, and P. G. Steeneken, "Nonequilibrium thermodynamics of acoustic phonons in suspended graphene," Phys. Rev. Res. **2**, 012058 (2020).

08 March 2024 14:14:06

© Author(s) 2024

[31] F. Ye, J. Lee, and P. X.-L. Feng, "Electrothermally tunable graphene resonators operating at very high temperature up to 1200 K," Nano Lett. **18**, 1678–1685 (2018).
[32] C.-H. Liu, I. S. Kim, and L. J. Lauhon, "Optical control of mechanical mode-coupling within a MoS_2 resonator in the strong-coupling regime," Nano Lett. **15**, 6727–6731 (2015).
[33] Z. Wang, R. Yang, and P. X.-L. Feng, "Thermal hysteresis controlled reconfigurable MoS_2 nanomechanical resonators," Nanoscale **13**, 18089–18095 (2021).
[34] S. Kim, J. Bunyan, P. F. Ferrari, A. Kanj, A. F. Vakakis, A. M. van der Zande, and S. Tawfick, "Buckling-mediated phase transitions in nano-electromechanical phononic waveguides," Nano Lett. **21**, 6416–6424 (2021).
[35] S. Rechnitz, T. Tabachnik, S. Shlafman, M. Shlafman, and Y. E. Yaish, "Dc signature of snap-through bistability in carbon nanotube mechanical resonators," Nano Lett. **22**, 7304–7310 (2022).
[36] A. Kanj, P. F. Ferrari, A. M. van der Zande, A. F. Vakakis, and S. Tawfick, "Ultra-tuning of nonlinear drumhead MEMS resonators by electro-thermoelastic buckling," Mech. Syst. Signal Process. **196**, 110331 (2023).
[37] N. Yamaki, K. Otomo, and M. Chiba, "Non-linear vibrations of a clamped circular plate with initial deflection and initial edge displacement, part I: Theory," J. Sound Vib. **79**, 23–42 (1981).
[38] C. Kim and S. Dickinson, "The flexural vibration of slightly curved slender beams subject to axial end displacement," J. Sound Vib. **104**, 170–175 (1986).
[39] H. Liu, G. Baglioni, C. B. Constant, H. S. van der Zant, P. G. Steeneken, and G. J. Verbiest, "Enhanced photothermal response near the buckling bifurcation in 2D nanomechanical resonators," arXiv:2305.00712 (2023).
[40] Y. Okada and Y. Tokumaru, "Precise determination of lattice parameter and thermal expansion coefficient of silicon between 300 and 1500 K," J. Appl. Phys. **56**, 314–320 (1984).
[41] X. Zhang, D. Sun, Y. Li, G.-H. Lee, X. Cui, D. Chenet, Y. You, T. F. Heinz, and J. C. Hone, "Measurement of lateral and interfacial thermal conductivity of single- and bilayer MoS_2 and $MoSe_2$ using refined optothermal Raman technique," ACS Appl. Mater. Interfaces **7**, 25923–25929 (2015).
[42] S. Sahoo, A. P. Gaur, M. Ahmadi, M. J.-F. Guinel, and R. S. Katiyar, "Temperature-dependent Raman studies and thermal conductivity of few-layer MoS_2," J. Phys. Chem. C **117**, 9042–9047 (2013).
[43] O. Çakıroğlu, N. Mehmood, M. M. Çiçek, A. Aikebaier, H. R. Rasouli, E. Durgun, and T. S. Kasırga, "Thermal conductivity measurements in nanosheets via bolometric effect," 2D Mater. **7**, 035003 (2020).
[44] E. H. Sondheimer, "The mean free path of electrons in metals," Adv. Phys. **50**, 499–537 (2001).
[45] J. Liu, G.-M. Choi, and D. G. Cahill, "Measurement of the anisotropic thermal conductivity of molybdenum disulfide by the time-resolved magneto-optic Kerr effect," J. Appl. Phys. **116**, 233107 (2014).
[46] J. L. Braun, C. H. Baker, A. Giri, M. Elahi, K. Artyushkova, T. E. Beechem, P. M. Norris, Z. C. Leseman, J. T. Gaskins, and P. E. Hopkins, "Size effects on the thermal conductivity of amorphous silicon thin films," Phys. Rev. B **93**, 140201 (2016).
[47] A. Arrighi, E. del Corro, D. N. Urrios, M. V. Costache, J. F. Sierra, K. Watanabe, T. Taniguchi, J. A. Garrido, S. O. Valenzuela, C. M. Sotomayor Torres, and M. Sledzinska, "Heat dissipation in few-layer MoS_2 and MoS_2/hBN heterostructure," 2D Mater. **9**, 015005 (2021).
[48] P. Norouzzadeh and D. J. Singh, "Thermal conductivity of single-layer WSe_2 by a Stillinger–Weber potential," Nanotechnology **28**, 075708 (2017).
[49] X. Liu, G. Zhang, Q.-X. Pei, and Y.-W. Zhang, "Phonon thermal conductivity of monolayer MoS_2 sheet and nanoribbons," Appl. Phys. Lett. **103**, 133113 (2013).
[50] Q. Cui, F. Ceballos, N. Kumar, and H. Zhao, "Transient absorption microscopy of monolayer and bulk WSe_2," ACS Nano **8**, 2970–2976 (2014).
[51] T. S. Kasirga, "Thermal conductivity measurements in 2D materials," in *Thermal Conductivity Measurements in Atomically Thin Materials and Devices* (Springer, 2020), pp. 11–27.
[52] A. Keşkekler, H. Arjmandi-Tash, P. Steeneken, and F. Alijani, "Symmetry-breaking-induced frequency combs in graphene resonators," Nano Lett. **22**, 6048–6054 (2022).
[53] G. Qin and M. Hu, "Thermal transport in phosphorene," Small **14**, 1702465 (2018).
[54] N. C. Frey, A. Bandyopadhyay, H. Kumar, B. Anasori, Y. Gogotsi, and V. B. Shenoy, "Surface-engineered MXenes: Electric field control of magnetism and enhanced magnetic anisotropy," ACS Nano **13**, 2831–2839 (2019).
[55] J. M. Park, Y. Cao, L.-Q. Xia, S. Sun, K. Watanabe, T. Taniguchi, and P. Jarillo-Herrero, "Robust superconductivity in magic-angle multilayer graphene family," Nat. Mater. **21**, 877–883 (2022).
[56] X. Wu and Q. Han, "Phonon thermal transport across multilayer graphene/hexagonal boron nitride van der Waals heterostructures," ACS Appl. Mater. Interfaces **13**, 32564–32578 (2021).
[57] W. Ren, Y. Ouyang, P. Jiang, C. Yu, J. He, and J. Chen, "The impact of interlayer rotation on thermal transport across graphene/hexagonal boron nitride van der Waals heterostructure," Nano Lett. **21**, 2634–2641 (2021).

08 March 2024 14:14:06

© Author(s) 2024